

A search for H I and OH absorption in $z \gtrsim 3$ CO emitters

S. J. Curran^{1,2,3*}, J. R. Allison^{2,4}, M. T. Whiting⁴, E. M. Sadler^{2,3}, F. Combes⁵,
M. B. Pracy², C. Bignell⁶ and R. Athreya⁷

¹*School of Chemical and Physical Sciences, Victoria University of Wellington, PO Box 600, Wellington 6140, New Zealand*

²*Sydney Institute for Astronomy, School of Physics, University of Sydney, NSW 2006, Australia*

³*ARC Centre of Excellence for All-sky Astrophysics (CAASTRO)*

⁴*CSIRO Astronomy and Space Science, PO Box 76, Epping NSW 1710, Australia*

⁵*l’Observatoire de Paris, 61 Av. de l’Observatoire F-75 014 Paris, France*

⁶*National Radio Astronomy Observatory, P.O. Box 2, Rt. 28/92 Green Bank, WV 24944-0002, USA*

⁷*Indian Institute of Science Education and Research, 900, NCL Innovation Park, Dr Homi Bhabha Road Pune, Maharashtra 411008, India*

Accepted —. Received —; in original form —

ABSTRACT

We present the results of a survey for H I 21-cm and OH 18-cm absorption in seven strong CO emitters at $z \gtrsim 3$. Despite reaching limits comparable to those required to detect 21-cm absorption at lower redshifts, we do not detect either transition in any of the objects searched. We believe that this is due to the high redshift selection causing all of our targets to have ultra-violet luminosities above the critical value, where all of the atomic gas in the host galaxy disk is suspected to be ionised. However, not only are all of our targets bright in CO emission, but detection of CO above the critical UV luminosity is generally not uncommon. This suggests that the molecular gas is shielded from the radiation or is physically remote from the source of the continuum emission, as it appears to be from CO observations of high redshift radio galaxies.

Key words: galaxies: active – quasars: absorption lines – galaxies: starburst – galaxies: evolution – galaxies: ISM – ultraviolet: galaxies

1 INTRODUCTION

Absorption of the background radio continuum by neutral hydrogen (H I) traces the cool component of the neutral gas in galaxies, the reservoir for star formation. High redshift observations of the 21-cm transition can address several pressing problems in cosmology and fundamental physics, such as the evolution of large-scale structure (e.g. Rawlings et al. 2004), detecting the Epoch of Re-ionisation (e.g. Carilli et al. 2004) and measuring the contribution of the neutral gas content to the mass density of the Universe (Kanekar et al. 2009; Curran 2010). Furthermore, spectral lines at high redshift can provide a measure of the values of the fundamental constants of nature at large look-back times (see Curran et al. 2004a). Of these, the hydroxyl radical (OH) is of particular interest since several different combinations of the constants can be measured from this single species (Darling 2003). That is, OH can potentially yield several measurements from a single sight-line, thus eliminating any relative velocity offsets which would cause a change in the redshifts, thus imitating a variation in the constants.

However, the detection of high redshift H I absorption is currently very elusive, with only three detections at $z \gtrsim 3$ (look-back times of $\gtrsim 11.5$ Gyr), two of which occur in galaxies interven-

ing the sight-lines to more distant quasars (Kanekar et al. 2007; Srianand et al. 2012) and one within the host galaxy of the quasar itself (Uson et al. 1991). The former “intervening” systems arise in damped Lyman- α absorption systems (DLAs)¹, with the low detection rate at high redshift being due to the geometry of an expanding Universe, where the high redshift cases cannot occult the background emission as effectively as those at lower redshift (Curran 2012). In the case of molecular absorption, the optical selection of targets means that the background quasi-stellar object (QSO) is not sufficiently obscured by the DLA (Curran et al. 2011a) to indicate a suitable environment for detecting molecular gas in absorption, either by OH (Curran et al. 2006) or by molecules with transitions in the millimetre band (e.g. CO, HCO⁺, HCN, Curran et al. 2011a). Thus, given that an optical redshift biases against a dusty, obscured object, in the millimetre and decimetre bands, the number of redshifted molecular absorption systems remains a paltry five, all of which are at a redshifts of $z \leq 0.89$ (Wiklind & Combes 1994, 1995, 1996b, 1998; Chengalur et al. 1999; Kanekar & Chengalur 2002; Kanekar et al. 2003, 2005).²

¹ Defined by their large neutral hydrogen column densities (in excess of $N_{\text{H I}} = 2 \times 10^{20} \text{ cm}^{-2}$), detected through the Lyman- α transition (usually redshifted into the optical band at $z \gtrsim 1.7$).

² Note, however, that the Lyman and Werner ultra-violet bands of H₂

* E-mail: Stephen.Curran@vuw.ac.nz

For the “associated” systems, the use of an optical redshift to which to tune the receiver also introduces a bias against the detection of neutral atomic and molecular gas, particularly at high redshift. From a survey for H I 21-cm and millimetre-band (CO, HCO⁺ & HCN) absorption at $z \gtrsim 3$, Curran et al. (2008b) obtained zero detections in the ten objects searched. Upon a detailed analysis of the photometry, they found all of the radio sources to be above a $\lambda = 912 \text{ \AA}$ luminosity of $L_{UV} \sim 10^{23} \text{ W Hz}^{-1}$, where 21-cm has *never* been detected, no matter the selection criteria or redshift (Curran et al. 2008b, 2011b, 2013a,b; Grasha & Darling 2011; Allison et al. 2012; Geréb et al. 2015; Aditya et al. 2016). This critical value applies at all redshifts (Curran & Whiting 2010) and, while 21-cm absorption is readily detected at $z \lesssim 1$ (e.g. Vermeulen et al. 2003), above these redshifts the optical selection of targets biases towards objects which are most UV luminous in the quasar rest-frame. In these, the H I ionising ($\lambda \leq 912 \text{ \AA}$) photon rate of $Q_{\text{HI}} \gtrsim 3 \times 10^{56} \text{ sec}^{-1}$ is sufficient to ionise *all* of the neutral atomic gas in a large spiral galaxy (Curran & Whiting 2012).

This suggests that even the Square Kilometre Array will not detect atomic or molecular absorption in the $z \gtrsim 3$ radio galaxies and quasars currently known (see figure 4 of Morganti et al. 2015). Thus, in order to find such absorption at high redshift, it is necessary to dispense with the traditional reliance upon optical redshifts and perform spectral scans towards optically faint radio sources. Currently, however, sufficiently wide spectral scans are subject to severe radio frequency interference (RFI).³ Therefore, in order to avoid the optical selection of targets, while retaining relatively narrow bandwidths, we can tune the receiver to the redshift of CO emission, which has been detected over 150 times at $z \gtrsim 0.1$. Here we present the results of the first survey for H I and OH absorption in a sample of $z \gtrsim 3$ CO emitters.

2 OBSERVATIONS AND ANALYSIS

2.1 Sample selection

From the known $z \gtrsim 0.1$ CO emitters⁴ we selected those for which the 21-cm transition is redshifted into the 90-cm bands of the Green Bank Telescope (GBT) and Giant Metrewave Radio Telescope (GMRT). As described in Curran et al. (2013a), we compiled

have been detected in 24 DLAs (compiled in Srianand et al. 2010 with the addition of Reimers et al. 2003; Fynbo et al. 2011; Guimarães et al. 2012; Srianand et al. 2012; Noterdaeme et al. 2015) although these have molecular abundances which are generally much lower than those detectable in the microwave band (Curran et al. 2004b, 2011a).

³ For example, 200 & 800 MHz wide scans for H I and OH with the Green Bank Telescope (see Tanna et al. 2013).

⁴ Compiled from Omont et al. (1996); Downes et al. (1999); Frayer et al. (1999); Papadopoulos et al. (2000); Cox et al. (2002); De Breuck et al. (2003a); Greve et al. (2003); Neri et al. (2003); Weiß et al. (2003); Baker et al. (2004); Hainline et al. (2004); De Breuck et al. (2005); Greve et al. (2005); Klammer et al. (2005); Kneib et al. (2005); Solomon & Vanden Bout (2005); Iono et al. (2006); Tacconi et al. (2006); Maiolino et al. (2007); Coppin et al. (2007); Willott et al. (2007); Ao et al. (2008); Casey et al. (2011); Daddi et al. (2009); Weiß et al. (2009); Bothwell et al. (2010); Daddi et al. (2010); Lestrade et al. (2010); Riechers et al. (2010); Combes et al. (2011); Danielson et al. (2011); Tacconi et al. (2010); Yan et al. (2010); Frayer et al. (2011); Riechers (2011); Emonts et al. (2011); Lupu et al. (2012); Magdis et al. (2012); Magnelli et al. (2012); Bauermeister et al. (2013); Combes et al. (2013); Bothwell et al. (2013); Saintonge et al. (2013); Tacconi et al. (2013); Emonts et al. (2014); Genzel et al. (2015).

the photometry⁵ and selected those with an appreciable radio flux (estimated to exceed $\approx 0.2 \text{ Jy}$ at the redshifted 21-cm frequency), prioritised by lowest $\lambda = 912 \text{ \AA}$ luminosity (Fig. 1). This yielded a shortlist of seven sources, of which six could be observed with the GBT and five with the GMRT. In order to offer some redundancy against RFI, we targeted the four sources which could be observed by both telescopes. Although we attempted to select the most optically faint sources, the high redshift ($z \gtrsim 3$) selection did nevertheless lead to the seven shortlisted sources having $\lambda = 912 \text{ \AA}$ luminosities above (but close to) the critical value of $L_{UV} \sim 10^{23} \text{ W Hz}^{-1}$ (see Table 3.1).

2.2 GMRT observations and analysis

Each of the sources was searched for H I 21-cm absorption on 30–31 August 2013 with the GMRT full 30 antenna array, using the 325 MHz receiver backed with the FX correlator over a bandwidth of 4 MHz. This was spread over 512 channels in orthogonal circular polarisations (LL & RR), giving a channel spacing of $\approx 7 \text{ km s}^{-1}$. For bandpass calibration 3C 48, 3C 147 and 3C 298 were used, with the phases being self calibrated apart from NVSS J012142+132058, which used 3C 49 and B2 2327+39. The data were flagged and reduced using the MIRIAD interferometry reduction package, with removal of the non-functioning antenna 18, leaving 406 baseline pairs. After averaging the two polarisations, a spectrum was extracted from the cube. Regarding each source:

0119+130 (NVSS J012142+132058) was observed for a total of 1.38 hours at a central frequency of 314.25 MHz. Flagging of the worst RFI left 342 baseline pairs. The source was unresolved by the $14.6'' \times 10.3''$ synthesised beam.

B2 0748+27 was observed for a total of 0.66 hours at a central frequency of 337.55 MHz. Only one baseline pair required flagging due to excessive RFI, although some ripple on the bandpass was still evident (Fig. 2). The source was unresolved by the $16.7'' \times 9.9''$ synthesised beam.

1359+154 (87GB 135911.5+152747) was observed for a total of 2.25 hours at a central frequency of 335.01 MHz. RFI was relatively severe, and flagging all baseline pairs above an r.m.s. noise level of 1 Jy, left just 127 pairs. The source was unresolved by the $29.1'' \times 16.0''$ synthesised beam.

1909+722 (4C+72.26) was observed for a total of 0.83 hours at a central frequency of 313.42 MHz, with only the flagging of one bad channel being required. The source was unresolved by the $19.7'' \times 12.3''$ synthesised beam.

B2 2327+39 was observed for a total of 1.47 hours at a central frequency of 346.95 MHz. The presence of a strong bandpass ripple required flagging of the worst affected baseline pairs, leaving 357. The source was unresolved by the $13.7'' \times 9.3''$ synthesised beam.

2.3 GBT observations and analysis

Each of the sources targeted with the GBT were observed for a total of two hours with the observations being completed over several sessions in 2013 (ending in October). For all observations, the

⁵ From the NASA/IPAC Extragalactic Database (NED) and matching the sources from the Wide-Field Infrared Survey Explorer (WISE), Two Micron All Sky Survey (2MASS) and GALEX databases.

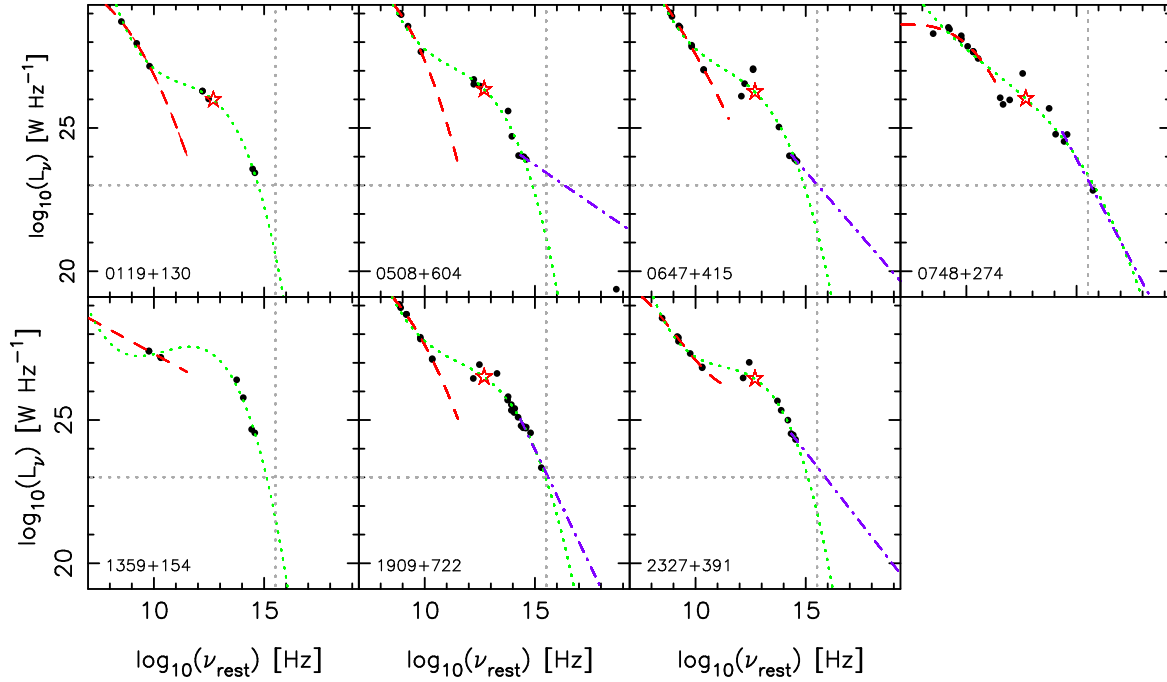


Figure 1. The rest-frame SEDs of our targets overlaid by fits to the photometry. The broken curve shows the third order polynomial fit to the radio data, the dotted curve the fit to all of the data (with the unfilled star showing the far infrared luminosity, $L_{\text{FIR}} \approx 5 - 14 \times 10^{12} L_{\odot}$, estimated from this) and the dash-dot line the power-law fit to the UV data, where possible (see Curran et al. 2013a for details). The vertical dotted line shows a rest-frame frequency of 3.29×10^{15} Hz ($\lambda = 912$ Å) and the horizontal line the “critical” UV luminosity of $L_{\text{UV}} = 10^{23}$ W Hz $^{-1}$.

Prime Focus 1 (PF1) receiver was used, backed by the GBT spectrometer, with a 12.5 MHz band over 4 098 or 8 196 lags. This gave a channel spacing of 3.052 or 1.526 kHz, corresponding to a spectral resolution of $\approx 1 - 3$ km s $^{-1}$, which was redressed to 10 km s $^{-1}$ after averaging the good scans.⁶ Four separate IFs were employed in two orthogonal linear polarisations (XX & YY), allowing us to observe both the H I 21-cm and OH 18-cm (main – 1665 & 1667 MHz, satellite – 1612 & 1720 MHz) lines simultaneously in cases where these were redshifted into the band (290–395 MHz).

Many of the observational scans were marred by RFI and those completely dominated by interference were removed. Nevertheless, there remained RFI spikes peppered throughout the band. Given that the GBT is a single dish telescope, thus not giving the option of removing badly affected baseline pairs, there was little we could do to improve the data, although we did apply the following steps:

- (i) We fitted and removed a low order polynomial to the band-pass, although some ripple was still apparent in some spectra (e.g. 0748+274, Fig. 2). We did not use high order polynomials in order to avoid over-fitting the data and thus possibly removing any putative broad, weak absorption features.
- (ii) Given that the detection of 21-cm emission at $z \gtrsim 0.2$ is beyond the capabilities of current radio telescopes (e.g. Catinella & Cortese 2015), any positive flux spikes were deemed to be caused by RFI. The noise levels and redshift ranges are quoted between these spikes (Table 3.1), where they bracket the expected absorption frequency (shown by the downwards arrows in Fig. 2).

(iii) Since we are searching for absorption, negative flux spikes cannot automatically be attributed to RFI, although most were similar in appearance to the positive flux spikes. We distinguished the RFI from any putative absorption features by:

- (a) Checking whether the features were dominant in some individual scans while being absent or frequency shifted in others. Often, as for the positive flux spikes, the spikes would be intermittent or dominated by a single scan (e.g. the 299 MHz feature in the H I bands of 0508+604 and 0647+415).
- (b) Checking if the feature resembles what we would expect. For example, for the “absorption” at 347.5 MHz towards 0647+415, we would expect a second feature separated by ≈ 0.4 MHz, due to the OH main-line doublet. Also, H I absorption is not apparent at the expected 296.0 MHz.
- (c) Checking if the feature is of the expected strength. For example, if the 381 MHz feature towards 1359+154 were real, we would expect the stronger main-line doublet to be apparent at ≈ 394 MHz, as well as H I absorption at 335.7 MHz, none of which are seen at these relatively clean frequencies.

Regarding the observation and data reduction for each individual target:

0508+604 (4C+60.07) was observed in four IFs for H I (centered on 296.66 MHz), the OH 1612 MHz line (336.72 MHz), the 1665 and 1667 MHz main lines in a single IF (redshifted to 347.83 and 348.24 MHz, respectively) and 1720 MHz (centred on 359.34 MHz). The H I band was very clean with 1.95 hours of integration on source remaining after flagging. In the final averaged spectrum there is a prominent absorption feature apparent at 298.73 MHz (blueshifted from the CO emission by 2060 km s $^{-1}$). However, the fact that this feature was not prominent in all scans, as well as being apparent as emission in two (out of 53 scans, as well as in the 0647+415 spectrum), leads us to conclude that this is instrumental

⁶ The line-widths of the current $z \gtrsim 0.1$ associated 21-cm detections range from 18 to 475 km s $^{-1}$, with a mean of 167 km s $^{-1}$ (Curran et al. 2013a).

in nature. The data were also relatively RFI-free in the other bands, leaving 1.91 hours on source for 1612 MHz, 1.83 hours for the OH main line band and 1.99 hours for the 1720 MHz band.

0647+415 (4C+41.17) was observed in four IFs for H I (centered on 296.16 MHz), the OH 1612 MHz line (336.16 MHz), the 1665 and 1667 MHz main lines in a single IF (redshifted to 347.25 and 347.66 MHz, respectively) and 1720 MHz (centred on 358.74 MHz). Flagging in the H I band left a total of 0.40 hours of integration on source, 0.52 hours for the OH 1612 MHz band, 0.55 hours for the OH main line band and 0.24 hours in the 1720 MHz band, in which all of the XX polarisation was lost. Note that the measured fluxes varied considerably between the two polarisations, particularly for the 1612 MHz band, where for XX this was ≈ 3 Jy, cf. ≈ 1 Jy in the YY, with the latter being the more consistent with the other bands and a flux density of ≈ 1.6 Jy being expected from a fit to the NED radio photometry.

B2 0748+27 was observed in two IFs for H I (centered on 337.55 MHz) and OH 1612 MHz (383.13 MHz). Some RFI was present, particularly in the lower frequency IF, and some flagging of the data was required. This left a total on source time of 0.68 hours for H I and 1.23 hours for OH, although some spikes still remained in the spectra (Fig. 2).

87GB 135911.5+152747 was observed in three IFs for H I (centered on 335.01 MHz), the OH 1612 MHz line (380.24 MHz) and the 1665 and 1667 MHz main lines in a single IF (redshifted to 392.78 and 393.25 MHz, respectively). After flagging of the worst RFI affected scans, the total on source integration times were 1.82 hours (H I), 0.92 hours (OH 1612 MHz) and 1.55 hours (OH main lines). For each scan a negative flux was noted in both polarisations. These are believed to be caused by confusion within the beam/sidelobes/off-position, due to the large beam ($\sim 40'$ at 335 MHz, Ries 2012).

1909+722 (4C+72.26) was observed in four IFs for H I (centered on 313.42 MHz), the OH 1612 MHz line (355.74 MHz), the 1665 and 1667 MHz main lines in a single IF (redshifted to 367.48 and 367.91 MHz, respectively) and 1720 MHz (centred on 379.64 MHz). Flagging left a total integration time of 1.51 hours in the H I band, 1.47 hours in the OH 1612 MHz band and 1.3 hours in the 1720 MHz OH band. RFI affected the middle of the main line OH band in the latter of two separate observing runs and flagging of this left 0.48 hours of integration time.

B2 2327+39 was observed in two IFs for H I (centered on 346.95 MHz) and OH 1612 MHz (393.80 MHz). After flagging of the worst RFI affected scans, leaving 1.19 hours of total integration time at the lower frequency, spikes were still present throughout the bandpass, which was clean between these (with an r.m.s. noise level of ≈ 4 mJy). Unfortunately, one of these lies at the frequency where the H I absorption is expected and so we do not quote an optical depth limit (Table 3.1). Spikes were all present at the higher frequency and, although close to the expected OH 1612 MHz absorption, 393.80 MHz is relatively clean, allowing us to quote a limit. Note that, the flux density at both frequencies varied between the two polarisations and two separate observing sessions and so the mean values quoted should not be deemed as reliable as that obtained from the interferometric (GMRT) observations.

3 RESULTS AND DISCUSSION

3.1 Observational results

In Fig. 2 we show the final spectra and summarise these in Table 3.1, from which we see neither H I nor OH were detected in any

of the targets. Since the OH absorption in the five known redshifted systems (Sect. 1) was detected on the basis of a previous H I absorption detection (Carilli et al. 1992, 1993, 1998; Chengalur et al. 1999; Kanekar & Briggs 2003), and that the absorption strength is only expected to be $\lesssim 10^{-4}$ times that of the 21-cm absorption (Curran et al. 2007), we will treat H I as a prerequisite for OH absorption and thus focus our discussion around the 21-cm results.

From Fig. 3, we see that our survey is as sensitive as many of the previous surveys for redshifted associated H I 21-cm absorption and deep enough to re-detect the majority of the known 21-cm absorbers.⁷ Therefore, we may expect ≈ 2 detections from our sample, or ≈ 7 from all the previous searches at $z \gtrsim 3$, based upon the 27% detection rate at $z \lesssim 3$. However, there is just one detection at $z \gtrsim 3$ (Uson et al. 1991), which is the only source below the critical UV luminosity (with $L_{UV} \approx 3 \times 10^{22}$ W Hz⁻¹). Due to all of our targets being at $z \gtrsim 3$, despite our best efforts, the UV luminosity of each of these was estimated to be close to the critical value of $L_{UV} \sim 10^{23}$ W Hz⁻¹. This is seen in Fig. 4, which shows the distribution for the H I 21-cm searches and the CO detections.⁸ From the figure it is clear that, while H I 21-cm is never detected above $L_{UV} \sim 10^{23}$ W Hz⁻¹ ($Q_{H I} \sim 10^{56}$ sec⁻¹), CO emission is detected in several cases, up to luminosities as high as $L_{UV} = 1.3 \times 10^{25}$ W Hz⁻¹ ($Q_{H I} = 1.2 \times 10^{59}$ sec⁻¹), which is over two orders of magnitude more luminous than the critical H I value.⁹ We now discuss possible reasons why CO emission is readily detected at ionising photon rates which are inhospitable to the neutral atomic gas.

3.2 Possible reasons for the presence of CO above the critical photo-ionising rate

3.2.1 Shielding by dust

Interstellar molecules form on dust grains and so shielding by dust may be a reason why CO is detected at ultra-violet luminosities which ionise the H I. However, the fact that the UV/visible fluxes are high may suggest that the sight-lines towards the sources have relatively low dust obscuration. In order to address this, in Fig. 5 we show the optical-near infrared colours of the CO emitters as a proxy for dust obscuration. From these, we see that the colours span a very similar range to optically selected QSOs (Schneider et al. 2007, which have a mean and a standard deviation of $\mu = 2.92$ and $\sigma = 0.75$, respectively) in comparison to $V - K \approx 5 - 9$ for the five known redshifted molecular absorption systems (see figure 1 of Curran et al. 2011a) and $V - K \gtrsim 2$ for associated 21-cm absorption (Curran & Whiting 2010).

⁷ Compiled from Mirabel (1989); van Gorkom et al. (1989); Uson et al. (1991); Carilli et al. (1992, 1998); Moore et al. (1999); Peck et al. (1999, 2000); Morganti et al. (2001); Ishwara-Chandra et al. (2003); Vermeulen et al. (2003); Curran et al. (2006); Gupta & Saikia (2006a); Gupta et al. (2006); Salter et al. (2010); Chandola et al. (2011); Curran et al. (2011b,c, 2013b); Geréb et al. (2015); Aditya et al. (2016) with the non-detections compiled in Curran & Whiting (2010).

⁸ UV luminosities and ionising photon rates could only be estimated for five of the targets, although the remaining two, 0119+130 & 1359+154, could have luminosities below the critical value (Fig. 1).

⁹ Unfortunately, the CO non-detections are generally not published, although of the eight non-detections of Emonts et al. (2014), rest-frame UV photometry exists for three, one of which has a luminosity above the critical value, with two below. Hence, like the incidence of H I 21-cm absorption, there must be another effect at play (e.g. gas disk orientation) in the detection of CO emission.

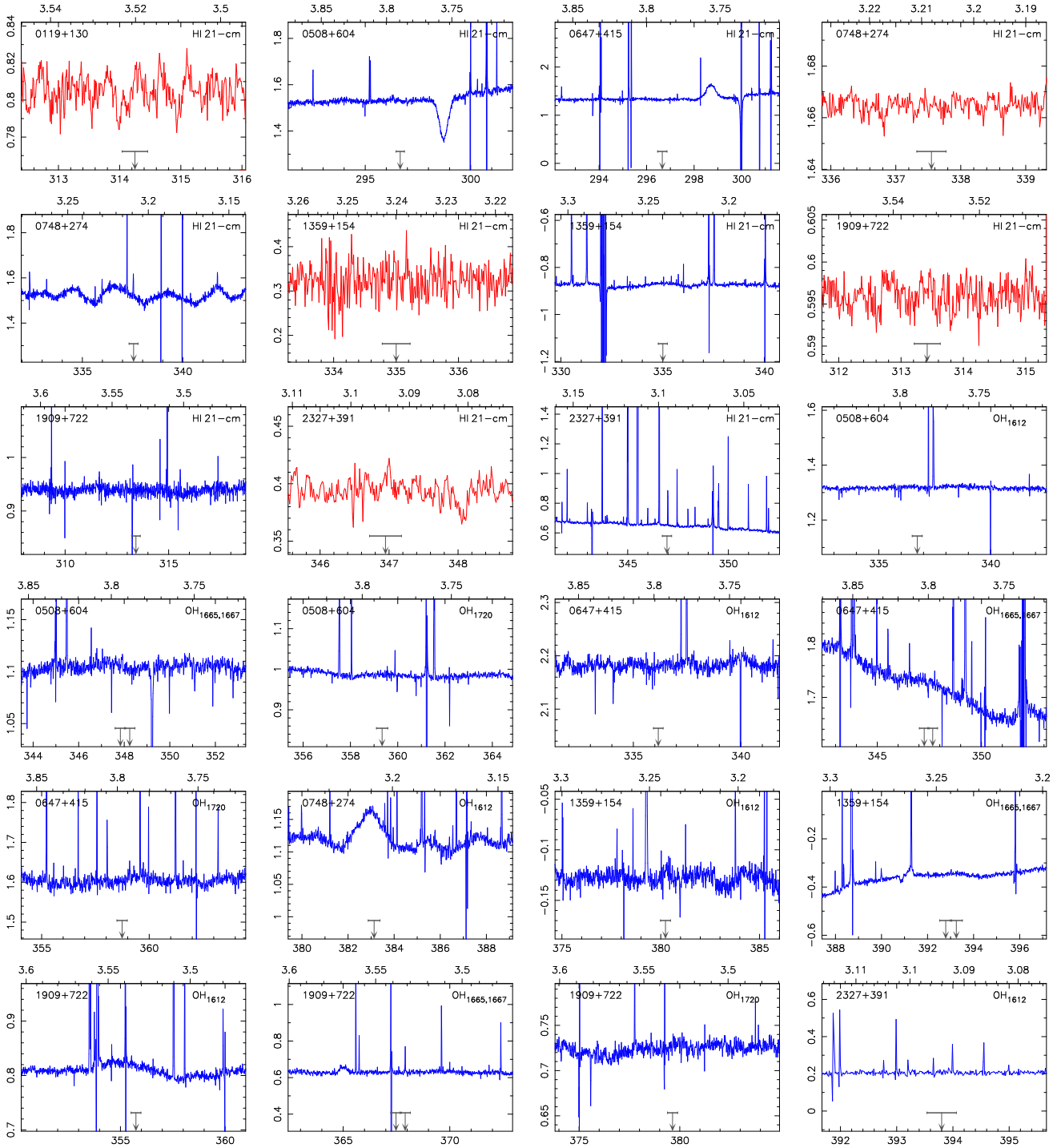


Figure 2. The final averaged H1, followed by the OH spectra (the 1665 & 1667 MHz main line spectra are shown in a single plot). The GBT spectra are shown in blue with the GMRT in red. The ordinate shows the flux density [Jy] and the abscissa the barycentric frequency [MHz] at a resolution of 10 km s^{-1} . The scale along the top axis shows the redshift for the appropriate transition (1667 MHz in the case of the OH main line spectra). The downwards arrow shows the expected frequency of the absorption from the CO redshift, with the horizontal bar showing a span of $\pm 200 \text{ km s}^{-1}$ for guidance.

The molecular absorption is due to low-excitation gas ($T_{\text{CMB}} \lesssim T_{\text{ex}} \lesssim 10 \text{ K}$, Wiklind & Combes 1995, 1996a,b, 1997), where the density is insufficient to populate the higher levels of the molecules, according to the higher kinetic temperatures (i.e. $T_{\text{kin}} \gg T_{\text{ex}}$). For gas in emission, however, both the volumetric density excitation temperature must be higher, although lower than the kinetic temperature ($T_{\text{kin}} \approx 50 - 100 \text{ K}$, cf. $T_{\text{ex}} \approx 13 \text{ K}$,

Papadopoulos et al. 2000, 2007), indicating that the gas is, on average, at intermediate densities and perhaps less obscured by dust, as is indicated by the less reddened colours.

However, the colours may not be a reliable indicator of the actual column densities, if the dense regions are embedded in a diffuse medium. Very dense self-shielded clumps of high column density gas could give rise to substantial CO emission with un-

Table 1 The limits obtained from our search for H I and OH absorption in $z \gtrsim 3$ CO emitters. z_{CO} and I_{CO} are the redshift and the integrated intensity of the CO ($J = 4 \rightarrow 3$) emission followed by the reference and the transition searched (in order of H I 21-cm, OH 1612, 1665, 1667 & 1720 MHz), where ν_{obs} is the central observing frequency based on the transition. σ_{rms} is the r.m.s. noise reached per 10 km s $^{-1}$ channel, between RFI spikes and after subtraction of a low order baseline, S_{cont} is the continuum flux density, $\tau_{3\sigma} \equiv -\ln(1 - 3\sigma_{\text{rms}}/S_{\text{cont}})$ is the optical depth limit calculated for a 10 km s $^{-1}$ channel. $N. (f/T)$ is the resulting column density of the respective species, where T is the spin temperature of the H I 21-cm line (T_{spin}) and N_{OH} , where T is the excitation temperature (T_{ex}), with f being the respective covering factor. z -range is the redshift range over which this is applicable (between the RFI spikes bracketing the line and/or excessive ripples in the bandpass). Lastly, we list the telescope used and the estimated (Fig. 1) $\lambda = 912$ Å luminosity.

NED Name	IAU Name	z_{CO}	I_{CO} [Jy km s $^{-1}$]	Ref	Trans.	ν_{obs} [MHz]	σ_{rms} [mJy]	S_{cont} [Jy]	$\tau_{3\sigma}$	$N. (f/T)$ [cm $^{-2}$]	z -range	Tel.	$\log_{10} L_{\text{UV}}$ [W Hz $^{-1}$]
NVSS J012142+132058	0119+130	3.520	1.20 ± 0.40	H04	H I	314.25	6.8	0.812	< 0.023	$< 4.2 \times 10^{17}$	3.493–3.547	GMRT	—
4C +60.07	0508+604	3.788	1.65 ± 0.35	P00	H I	296.66	6.7	1.527	< 0.013	$< 2.4 \times 10^{17}$	3.763–3.809	GBT	23.08
...	OH ₁₆₁₂	336.72	6.9	1.317	< 0.016	$< 3.6 \times 10^{14}$	3.782–3.798
...	OH ₁₆₆₅	347.83	6.0	1.105	< 0.016	$< 6.9 \times 10^{13}$	3.771–3.820
...	OH ₁₆₆₇	348.24	$< 3.8 \times 10^{13}$	3.777–3.826
...	OH ₁₇₂₀	359.34	8.2	0.984	< 0.025	$< 5.2 \times 10^{14}$	3.764–3.805
4C +41.17	0647+415	3.796	1.20 ± 0.15	D05	H I	296.16	12.8	1.333	< 0.029	$< 5.3 \times 10^{17}$	3.779–3.807	GBT	23.20
...	OH ₁₆₁₂	336.16	11.1	2.181	< 0.015	$< 3.3 \times 10^{14}$	3.782–3.838
...	OH ₁₆₆₅	347.25	15.6	1.723	< 0.027	$< 1.2 \times 10^{14}$	3.779–3.842
...	OH ₁₆₆₇	347.66	$< 6.4 \times 10^{13}$	3.784–3.847
...	OH ₁₇₂₀	358.74	11.0	1.612	< 0.021	$< 4.4 \times 10^{14}$	3.786–3.804
B2 0748+27	0748+274	3.208	5.96 ± 0.45	H04	H I	337.55	3.1	1.665	< 0.006	$< 1.0 \times 10^{17}$	3.188–3.219	GMRT	23.26
...	8.9	1.527	< 0.046	$< 8.5 \times 10^{17}$	3.138–3.279	GBT	...
...	OH ₁₆₁₂	383.13	18.5	1.137	< 0.049	$< 1.1 \times 10^{15}$	3.187–3.228
87GB 135911.5+152747	1359+154	3.240	2.50 ± 0.40	R11	H I	335.01	38	0.323	< 0.44	$< 8.0 \times 10^{18}$	3.216–3.264	GMRT	—
...	H I	...	7.2	—	$< 0.067^a$	$< 1.2 \times 10^{18}$	3.229–3.250	GBT	...
...	OH ₁₆₁₂	380.24	13.1	—	$< 0.12^a$	$< 2.6 \times 10^{15}$	3.202–3.249
...	OH ₁₆₆₅	392.78	6.7	—	$< 0.062^a$	$< 2.6 \times 10^{14}$	3.208–3.254
...	OH ₁₆₆₇	393.25	$< 1.5 \times 10^{14}$	3.213–3.260
4C +72.26	1909+722	3.532	1.62 ± 0.30	P00	H I	313.42	1.7	0.594	< 0.009	$< 1.6 \times 10^{17}$	3.506–3.546	GMRT	23.11
...	H I	...	8.1	0.956	< 0.025	$< 4.6 \times 10^{17}$	3.511–3.535	GBT	...
...	OH ₁₆₁₂	355.74	5.1	0.806	< 0.019	$< 4.2 \times 10^{14}$	3.511–3.537
...	OH ₁₆₆₅	367.48	13.9	0.732	< 0.057	$< 2.4 \times 10^{14}$	3.508–3.533
...	OH ₁₆₆₇	367.91	$< 1.4 \times 10^{14}$	3.513–3.538
...	OH ₁₇₂₀	379.64	17.2	0.720	< 0.072	$< 1.5 \times 10^{15}$	3.484–3.536
B2 2327+39	2327+391	3.094	1.30 ± 0.30	D03	H I	346.95	8.1	0.395	$< 0.062^b$	$< 1.1 \times 10^{18}$	3.083–3.109	GMRT	23.37
...	H I	...	3.8	0.655	< 0.017	$< 3.2 \times 10^{17}$	3.094–3.098	GBT	...
...	OH ₁₆₁₂	393.80	7.3	0.210	< 0.010	$< 2.2 \times 10^{14}$	3.075–3.116

References: P00 – Papadopoulos et al. (2000), D03 – De Breuck et al. (2003), H04 – Hainline et al. (2004), D05 – De Breuck et al. (2005), R11 – Riechers (2011).

Notes: ^aBased upon the GMRT 335 MHz flux measurement. ^bDe Breuck et al. (2003) also searched for H I 21-cm absorption with the Westerbork Synthesis Radio Telescope (WSRT), obtaining $\tau_{3\sigma} < 0.013$ (from $S_{\text{cont}} = 0.405$ Jy), although the channel width is not published.

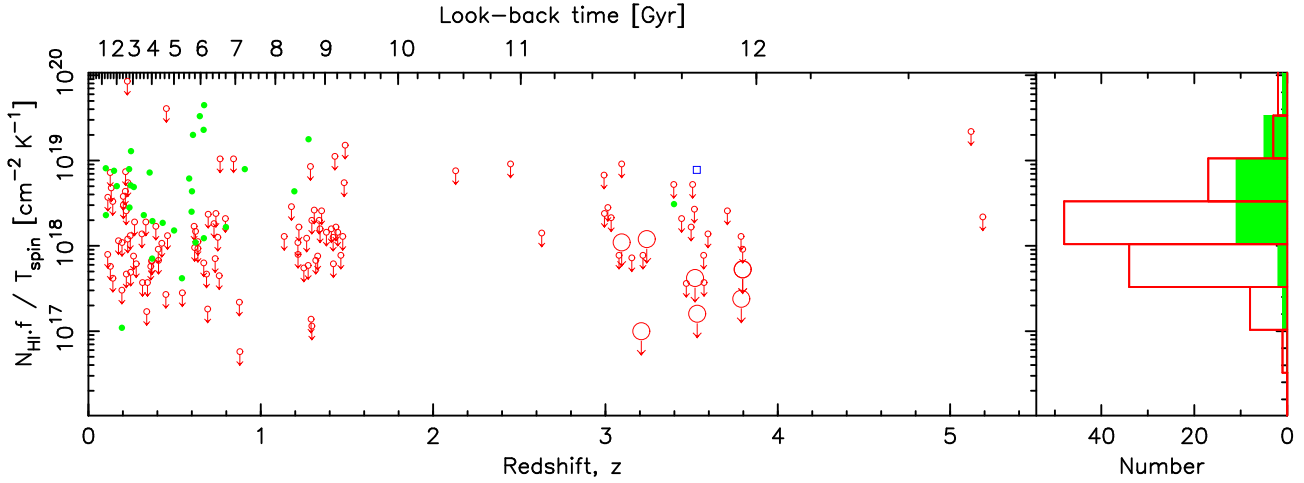


Figure 3. The line strength ($1.823 \times 10^{18} \int \tau dv$) versus redshift for the $z \geq 0.1$ H I 21-cm absorption searches. The filled circles/histogram represent the detections and the unfilled circles/histogram the 3σ upper limits to the non-detections, where the large circles signify the CO emitters searched for 21-cm absorption. The unfilled square at $z = 3.53$ shows the tentative detection of Aditya et al. (2016), which we will treat as a non-detection until confirmed.

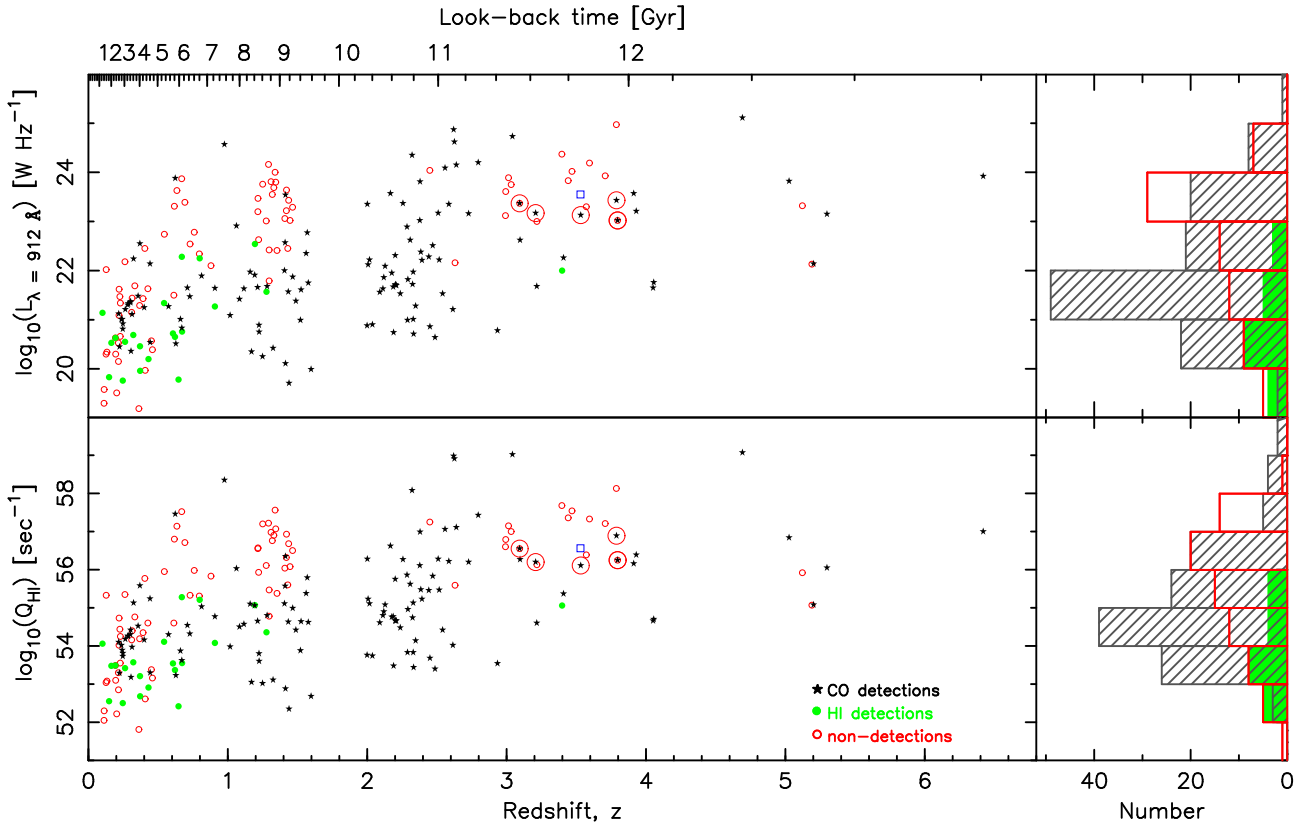


Figure 4. The $\lambda = 912 \text{ \AA}$ continuum luminosity (top) and ionising ($\lambda \leq 912 \text{ \AA}$) photon rate (bottom) versus redshift for the sources detected in CO emission (filled stars) in addition to those searched in H I 21-cm absorption (filled circles - detections, unfilled circles - non-detections, where the large circles signify the CO emitters searched). Again, the unfilled square shows the tentative detection of Aditya et al. (2016), where $L_{UV} = 3.5 \times 10^{23} \text{ W Hz}^{-1}$ and $Q_{H I} = 3.6 \times 10^{56} \text{ sec}^{-1}$. The hatched histogram shows the distribution for the CO emitters, the filled the 21-cm detections and the unfilled the non-detections.

reddened colours, if the surface filling factor of the dense gas is low. These low filling factors ($\lesssim 1\%$ in absorption, Pfenninger & Combes 1994; Pfenninger et al. 1994) offer an alternate explanation to the lack of 21-cm absorption. However, as seen from Fig. 3, 21-cm absorption is readily detected at $z \lesssim 1$ and is also detected in all five of the decimetre/millimetre band molecular absorbers (Carilli et al.

1992, 1993, 1998; Chengalur et al. 1999; Kanekar & Briggs 2003) and so low filling factors are unlikely to be the cause of the 21-cm non-detections.

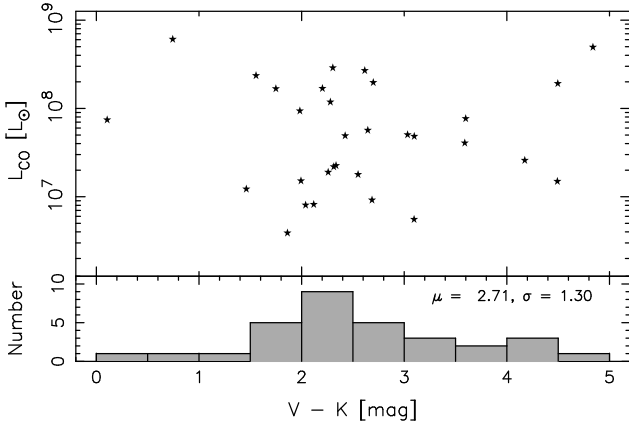


Figure 5. The luminosity of the CO emission versus the optical–near infrared colours of the CO emitters, for which both V and K magnitudes are available.

3.2.2 Self-shielding

Another viable reason for the detection of CO at UV luminosities unfavourable to 21-cm absorption is the possibility that the molecular gas is self-shielded, due to its higher density. Curran & Whiting (2012) showed that an ionising photon rate of $Q_{\text{H I}} \sim 10^{56} \text{ sec}^{-1}$ was sufficient to ionise all of the neutral gas in a galaxy with the H I distribution of the Milky Way (Kalberla & Kerp 2009). This critical value is therefore valid for a central gas density of $n_0 \approx 10 \text{ cm}^{-3}$, which decays with galactocentric radius with a scale-length of $R = 3 \text{ kpc}$. However, CO traces gas of significantly higher density, and applying the canonical $n_0 \sim 10^3 \text{ cm}^{-3}$ to the maximum luminosity at which CO is detected, $L_{\text{UV}} = 1.3 \times 10^{25} \text{ W Hz}^{-1}$, gives a scale-length of $R \approx 500 \text{ pc}$ and a total gas mass of $M_{\text{gas}} = \int_0^R \rho dV = 4 \times 10^9 M_{\odot}$, both values being typical of a spiral galaxy (e.g. Curran et al. 2008a).

However, while an exponential disk may reasonably model the large-scale neutral atomic gas distribution in a galaxy, the denser molecular gas is expected to be embedded in discrete clouds within this. This could mean that the molecular gas is shielded by the enveloping atomic gas (e.g. Krumholz et al. 2008, 2009; McKee & Krumholz 2010), since the dissociation of H_2 requires higher energy photons than the ionisation of H I (14.7 cf. 13.6 eV, Spitzer 1948).¹⁰ Because of its large dipole moment, it is CO, not H_2 directly, which is detected in these millimetre band surveys and so it is possible that CO emission at high redshift could arise in very different environments than in the Galaxy, and use of the Galactic conversion ratio (Strong et al. 1988) would not be warranted. Therefore, since we have no direct measure of the H_2 emission properties of these objects, it is more prudent to consider the CO directly. This is dissociated at 11.09 eV (e.g. Visser et al. 2009), which would suggest that the CO actually shields the H I, and being readily detected, while H I is not, this would indicate that the CO may be more remote from the AGN activity, a possibility which we now discuss.

3.2.3 CO remote from the UV continuum

CO emission in high redshift galaxies has been observed to extend to large scales; $\gtrsim 10 \text{ kpc}$ in the $4 \rightarrow 3$ transition

¹⁰ Since H_2 is homo-nuclear it has no dipole moment, making the dissociation of H_2 by 4.52 eV photons forbidden.

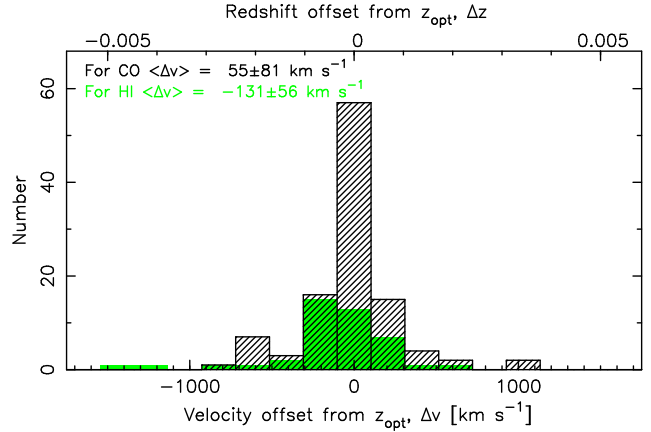


Figure 6. The velocity offset from the systemic for the CO emission (hatched histogram) and H I absorption (coloured histogram) detections.

(Papadopoulos et al. 2000; Ivison et al. 2012) and $\gtrsim 50 \text{ kpc}$ in the $1 \rightarrow 0$ transition. This extended emission appears to arise from external components such as merging gas-rich galaxies (De Breuck et al. 2003b,a, 2005; Emonts et al. 2013) and $\text{Ly}\alpha$ halos around the host galaxy (Nesvadba et al. 2009). Furthermore, the CO emission is often aligned with the radio jet axis (Klamer et al. 2004; Nesvadba et al. 2009), which is a further indication that the CO is not confined to the host radio galaxy.

Since the H I absorption is believed to arise in the disk, if not the obscuring nuclear material (Curran & Whiting 2010), the molecular gas detected in emission may therefore be spatially offset from the atomic detected in absorption. If this were the case, we may expect differences in the offsets of each species from the systemic redshift. Calculating these via

$$\Delta v = c \frac{(\Delta z + 1)^2 - 1}{(\Delta z + 1)^2 + 1} \approx c \Delta z, \text{ where } \Delta z = \frac{z_{\text{opt}} + 1}{z_{\text{CO, H I}} + 1} - 1,$$

gives mean offsets of $\langle \Delta v \rangle = 55 \pm 81 \text{ km s}^{-1}$ for the CO emission and $\langle \Delta v \rangle = -131 \pm 56 \text{ km s}^{-1}$ for the H I absorption (Fig. 6). That is, on average, the H I absorption may be more offset from the systemic velocity, where we would expect this to be less, if the H I were intrinsic. A Kolmogorov-Smirnov test of the Δv values gives a probability of 9.81×10^{-3} that the two samples are drawn from the same population, which is significant at 2.58σ assuming Gaussian statistics (Fig. 8).

This overall blueshift of the cool neutral gas was also noted by Vermeulen et al. (2003), whose sample comprises 19 of the 43 H I absorbers for which we can estimate Δv . The blueshift was attributed to outflowing gas (e.g. Morganti et al. 2015 and references therein) and fast outflows could account for the offsets of $\Delta v \gtrsim 500 \text{ km s}^{-1}$, which exceed the escape velocity of a large spiral galaxy. Fast outflowing gas is predominant in compact radio sources (e.g. Vermeulen et al. 2003; Geréb et al. 2015), which may have higher H I detection rates than in the extended sources (e.g. Pihlström et al. 2003; Gupta & Saikia 2006b). Since such kinetic feedback can deplete the hydrogen in galaxies (e.g. Dasyra & Combes 2012; Ciccone et al. 2014; Aalto et al. 2016), the depletion of gas in more mature (extended) objects could explain the paucity of 21-cm absorption detections, although high resolution radio imaging of the CO emitters would be required in order to verify this. Note, however, that once the $L_{\text{UV}} \sim 10^{23} \text{ W Hz}^{-1}$ sources are removed from the radio source samples, the H I detection rates in compact objects does not differ significantly from

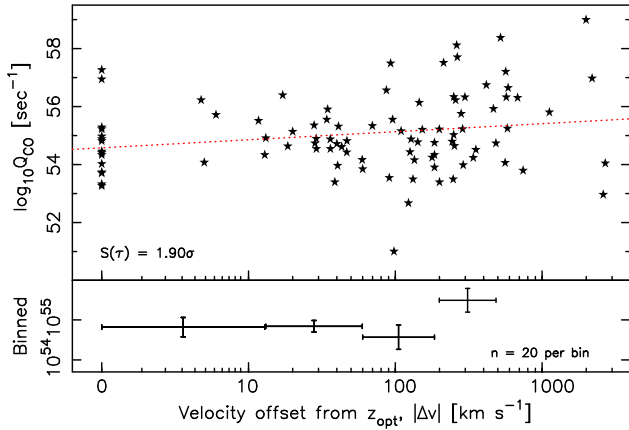


Figure 7. The CO photo-dissociation rate versus the absolute velocity offset from the systemic for the CO emission. Q_{CO} is obtained from the SED fits at $\lambda \leq 1119 \text{ \AA}$, cf. $\lambda \leq 912 \text{ \AA}$ for H I , where possible.

those in non-compact objects, which is consistent with the compact objects being less mature and luminous than the non-compact sources (Curran & Whiting 2010; Allison et al. 2012). Thus, we believe that photo-ionisation of the neutral gas remains a key factor in the non-detection of H I .

Furthermore, in drawing any conclusions from the velocity offsets, it should be noted that many of the optical redshifts are only accurate to the second decimal place giving uncertainties of $\sim 10^2 \text{ km s}^{-1}$ and so the absolute value of Δv may be unreliable, with many of the $\Delta v = 0$ values arising by default (see Fig. 7). The narrower spread in H I offsets¹¹ may suggest that the atomic gas is more likely to be associated with the radio source, although one can not draw any firm conclusions from the distribution of the offsets until more accurate optical redshifts become available.

Returning to the dissociation of CO by the UV flux, in Fig. 7 we show the CO photo-dissociation rate versus Δv , from which we only see a weak correlation. Assuming that this is diluted by inaccurate optical redshifts and projection effects, and provided that Δv is a reliable proxy for the distance between the AGN host, this may be evidence of the molecular clouds being able to survive larger rates ($Q_{\text{CO}} \gg 10^{56} \text{ sec}^{-1}$) due to their larger distances from the AGN.

3.2.4 UV continuum arising from star formation

Another possibility for the detection of CO emission in the brightest UV sources, is that both luminosities are correlated with star forming activity: Due to the low efficiency of star-formation, the consumption of molecular gas is far from complete, with a depletion times of $2 - 3 \text{ Gyr}$ at $z = 0$ (Bigiel et al. 2008) compared to 0.7 Gyr at $z = 1 - 3$ (Tacconi et al. 2013). That is, there is an apparent increase in star formation efficiency with redshift.

Investigating the origin of the UV luminosity, in Fig. 8 we show the CO line luminosity versus the UV continuum luminosity, from which a non-parametric generalised Kendall-tau test gives a $P(\tau) = 1.5 \times 10^{-8}$ probability of the observed correlation occurring by chance, which is significant at 5.66σ . Such a relationship may be expected, since far-infrared emission is a tracer of

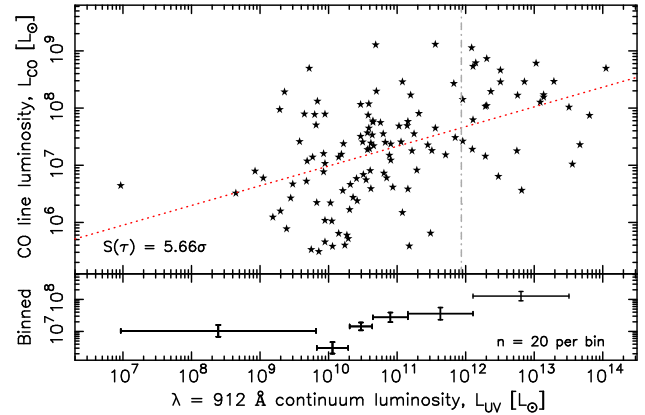


Figure 8. The CO line versus the UV continuum luminosity for the CO emitters for which this can be determined (see Curran et al. 2013a). The vertical broken line at $L_{\text{UV}} = 8.6 \times 10^{11} L_{\odot}$ shows $L_{\text{UV}} = 10^{23} \text{ W Hz}^{-1}$ and the dotted line the fit to all of the points.

the star formation rate (SFR) in Ultra Luminous Infrared Galaxies (ULIRGS, where $L_{\text{FIR}} \gtrsim 10^{12} L_{\odot}$, e.g. Kennicutt 1998) and six of our sample are estimated to have $L_{\text{FIR}} \approx 5 - 14 \times 10^{12} L_{\odot}$ (Fig. 1). The fact that they have both high CO and FIR luminosities, suggests that they are host to high star formation rates (e.g. Freundlich et al. 2013; Genzel et al. 2015). However, it is generally assumed that all of the FIR emission arises from star formation and such a large dynamic range may be subject to selection effects, such as an increasing luminosity with redshift probing differing host morphologies and amplification of the flux by gravitational lensing.¹²

In Fig. 9, we also find a strong correlation between the radio and UV continuum luminosities ($P(\tau) = 7.32 \times 10^{-6}$ for the 27 sources for which the radio luminosity can be obtained). Since the radio-FIR correlation is often attributed to star-formation, this could strengthen the argument that the high UV luminosities arise from star formation, although the radio-FIR relationship is generally limited to $L_{\text{radio}} \lesssim 10^{24} \text{ W Hz}^{-1}$ (e.g. Sanders & Mirabel 1996; Basu et al. 2015; Pannella et al. 2015). Furthermore, at $L_{\text{radio}} \gtrsim 10^{23} \text{ W Hz}^{-1}$, the population rapidly becomes dominated by AGN (e.g. Mauch & Sadler 2007), although this is only measured to $z \lesssim 0.3$ and it is not known how this extrapolates to high redshift.

In Fig. 10 we show the estimated star formation rates, based upon the UV ($\lambda = 1500 \text{ \AA}$) luminosities (Madau et al. 1998). The maximum $L_{\lambda=1500 \text{ \AA}} = 3.5 \times 10^{23} \text{ W Hz}^{-1}$ at which 21-cm is detected corresponds to a SFR of $430 M_{\odot} \text{ yr}^{-1}$, with the maximum $L_{\lambda=1500 \text{ \AA}} = 1.4 \times 10^{25} \text{ W Hz}^{-1}$ at which CO is detected corresponding to $17000 M_{\odot} \text{ yr}^{-1}$. By assuming that all of the FIR emission is due to star formation, rates of $3000 M_{\odot} \text{ yr}^{-1}$ have been found in high redshift ($z \gtrsim 6$) CO emitters (e.g. Bertoldi et al. 2003), although these rates are believed to occur in short bursts ($< 10 \text{ Myr}$). Thus, we obtain extremely high star formation rates based upon the UV luminosities of the CO emitters and hence believe that, at least partially, the high luminosities, and subsequent dust heating, are caused by increased AGN activity (e.g. Genzel & Cesarsky 2000).

One way to address the origin of the UV radiation would be through spectral classification, although, of the six of the seven

¹¹ An F-test rejects the null hypothesis of equal variances in the H I and CO samples at a very high significance (a p -value of 6.65×10^{-9}).

¹² Of our sample, 0748+27 and 1359+154 are known to be lensed.

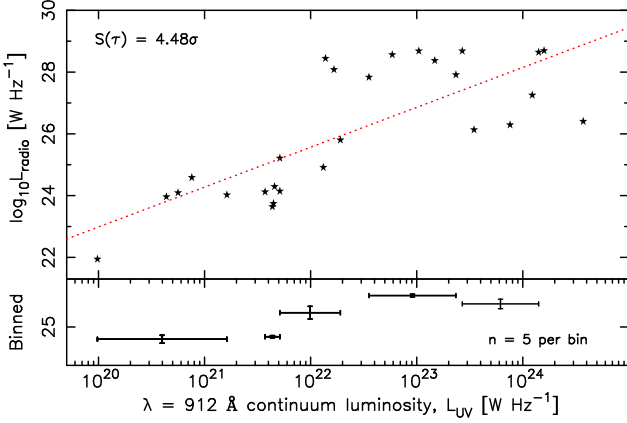


Figure 9. The 1.4 GHz radio continuum versus that of the UV for the CO emitters, where available. For the $z \gtrsim 0.1$ associated 21-cm absorbers, the radio powers are typically $L_{\text{radio}} \gtrsim 10^{26} \text{ W Hz}^{-1}$ (Curran et al. 2008b, or $\int L_{\text{radio}} d\nu \gtrsim 10^{35} \text{ W}$, Curran et al. 2013b).

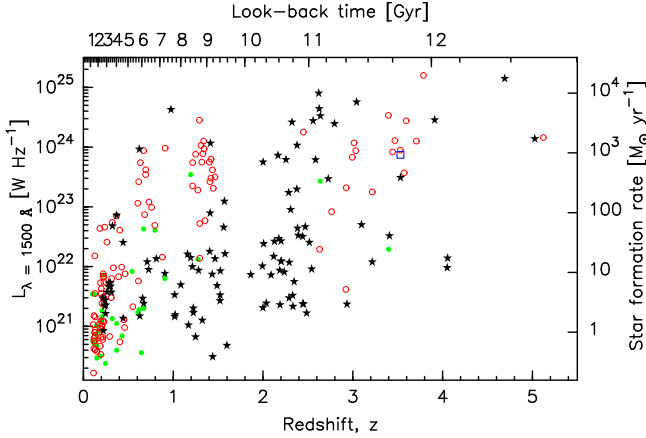


Figure 10. The rest-frame $\lambda = 1500 \text{ \AA}$ luminosity of the CO emitters (stars) and 21-cm absorption searches (circles), where the right axis shows the star formation rate derived from $\text{SFR} = L_{\lambda=1500 \text{ \AA}} / 8.0 \times 10^{20}$ (Madau et al. 1998).

target spectra which could be found, all are UV (rest) emission line spectra, with little continuum, and so are difficult to classify. However, NED classifies three as QSOs (0748+27, 1359+154 & 2327+39) and four as galaxies (0119+130, 0508+604, 0647+415 & 1909+722), although the 50% detection rate in both type-1 and type-2 objects (Curran & Whiting 2010) suggests that the host morphology makes little difference to the detection of 21-cm absorption in objects below the critical UV luminosity.

4 SUMMARY

We have undertaken a survey for atomic (H I 21-cm) and molecular (OH 18-cm) absorption in seven strong CO emitters at $z \gtrsim 3$. Our motivation was to circumvent the need for an optical redshift, to which to tune the receiver, which selects against the detection of decimetre absorption at high redshift. Tuning to the CO redshift also has the advantage that large amounts ($\gtrsim 10^{10} M_{\odot}$) of molecular gas (e.g. De Breuck et al. 2003a; Solomon & Vanden Bout 2005) are known to exist and H I absorption and CO emission are often coincident in low- z active galactic nuclei (e.g. Curran et al.

1999, cf. Koribalski 1996 and Curran et al. 2001, cf. Ables et al. 1987). Despite this, no absorption of either species was detected. We attribute this as being due to the targets, despite careful selection, having rest-frame ultra-violet luminosities close to the value above which all of the neutral gas is ionised (Curran & Whiting 2012).

While the non-detection of H I 21-cm absorption within the host galaxies of sources with ionising photon rates exceeding $Q_{\text{H I}} \approx 3 \times 10^{56} \text{ sec}^{-1}$ ($L_{\text{UV}} \gtrsim 10^{23} \text{ W Hz}^{-1}$) appears to be a universal phenomenon, holding true for various heterogeneous and unbiased samples, with varying selection criteria and over all redshifts, we find that CO emission is readily detected at $L_{\text{UV}} \gg 10^{23} \text{ W Hz}^{-1}$. In order to explain the detection of molecular gas in emission, while atomic gas in absorption remains undetected, we suggest the following, non-mutually exclusive, possibilities:

(i) That, due to the ionisation of H I occurring at a lower energy than the dissociation of H_2 , as per Galactic clouds, the molecular gas is shielded by the atomic gas. However, by the same argument the CO should shield the H I, although this is likely to be embedded in dense molecular cores which are enveloped by the more diffuse atomic gas.

(ii) CO traces higher density gas ($n_{\text{H}_2} \gtrsim 10^3 \text{ cm}^{-3}$, cf. $n_{\text{H I}} \sim 10 \text{ cm}^{-3}$ for H I), which could provide the CO with better self-shielding against the UV flux. From our model galaxy (Curran & Whiting 2012), we find that the maximum luminosity at which CO is detected ($L_{\text{UV}} = 1.3 \times 10^{25} \text{ W Hz}^{-1}$) gives a gas density distribution and mass which is consistent with the molecular gas in a typical spiral galaxy. This, however, relies on the assumption that the distribution of CO is spatially coincident with the H I, when the molecular gas is likely to be embedded in discrete clumps.

(iii) The CO gas is located in a dustier environment which provides better shielding against photo-ionisation. This appears to be the case for both molecular and H I 21-cm absorption which are correlated with the optical–near infrared colours of the sight-line. For the CO emission, however, no correlation is seen and this is readily detected at colours which are similar to those of optically selected QSOs, ($V - K \lesssim 5$), whereas CO absorption has thus far only been detected towards much redder sight-lines ($V - K \gtrsim 5$). This suggests either that dust does not play as an important role in CO emission as in absorption or that the CO is physically offset from the sight-line (to the radio/UV source) along which the colours are measured.

(iv) At high redshift, there is evidence that the CO emission is physically remote from the source of the continuum emission, meaning that the CO is subject to much lower UV fluxes than the cool, neutral gas located within the host galaxy.

We also investigate the possibility that the UV emission arises primarily from star formation, as may be evident through a strong correlation between the UV and CO luminosities. However, it is not clear how much of the ultra-violet emission is due to nuclear activity in these objects, although three of our seven targets appear to be QSOs and all seven have radio luminosities typical of AGN. Thus, it is possible that a large fraction of UV emission does not arise from star formation and that the presence of CO in these UV luminous sources could be explained by self-shielding of the molecular gas or their distance from the continuum source.

Whatever the cause, the detection of H I and OH absorption at high redshift remains elusive, with wide-band decimetre-wave spectral scans of optically obscured objects being required to detect these tracers of cool gas at high redshift and perhaps shed light

upon the paucity of the star forming reservoir in the locale of warm molecular gas.

ACKNOWLEDGEMENTS

We wish to thank Bjorn Emonts for his valuable input as well as the staff of the GBT and GMRT that made these observations possible. The GMRT is run by the National Centre for Radio Astrophysics of the Tata Institute of Fundamental Research. The National Radio Astronomy Observatory is a facility of the National Science Foundation operated under cooperative agreement by Associated Universities, Inc. This research has made use of the NASA/IPAC Extragalactic Database (NED) which is operated by the Jet Propulsion Laboratory, California Institute of Technology, under contract with the National Aeronautics and Space Administration and NASA's Astrophysics Data System Bibliographic Service. This research was conducted by the Australian Research Council Centre of Excellence for All-sky Astrophysics (CAASTRO), through project number CE110001020.

REFERENCES

- Aalto S. et al., 2016, A&A, submitted (arXiv:1510.08827)
- Ables J. G., Foster J. R., and P. T. Rayner R. N. M., Whiteoak J. B., Mathewson D. S., Kalnajs A. J., Peters W. L., Wehner H., 1987, MNRAS, 226, 157
- Aditya J. N. H. S., Kanekar N., Kurapati S., 2016, MNRAS, 455, 4000
- Allison J. R. et al., 2012, MNRAS, 423, 2601
- Ao Y., Weiß A., Downes D., Walter F., Henkel C., Menten K. M., 2008, A&A, 491, 747
- Baker A. J., Tacconi L. J., Genzel R., Lehnert M. D., Lutz D., 2004, ApJ, 604, 125
- Basu A., Wadadekar Y., Beelen A., Singh V., Archana K. N., Sirothia S., Ishwara-Chandra C. H., 2015, ApJ, 803, 51
- Bauermeister A., Blitz L., Bolatto A., Bureau M., Teuben P., Wong T., Wright M., 2013, ApJ, 763, 64
- Bertoldi F. et al., 2003, A&A, 409, L47
- Bigiel F., Leroy A., Walter F., Brinks E., de Blok W. J. G., Madore B., Thornley M. D., 2008, AJ, 136, 2846
- Bothwell M. S. et al., 2010, MNRAS, 405, 219
- Bothwell M. S. et al., 2013, MNRAS, 429, 3047
- Carilli C. L., Gnedin N., Furlanetto S., Owen F., 2004, Science with the Square Kilometer Array, New Astronomy Reviews 48, Carilli C. L., Rawlings S., eds., Elsevier, Amsterdam, pp. 1053–1061
- Carilli C. L., Menten K. M., Reid M. J., Rupen M. P., Yun M. S., 1998, ApJ, 494, 175
- Carilli C. L., Perlman E. S., Stocke J. T., 1992, ApJ, 400, L13
- Carilli C. L., Rupen M. P., Yanny B., 1993, ApJ, 412, L59
- Casey C. M. et al., 2011, MNRAS, 415, 2723
- Catinella B., Cortese L., 2015, MNRAS, 446, 3526
- Chandola Y., Sirothia S. K., Saikia D. J., 2011, MNRAS, 418, 1787
- Chengalur J. N., de Bruyn A. G., Narasimha D., 1999, A&A, 343, L79
- Cicone C. et al., 2014, A&A, 562, A21
- Combes F., García-Burillo S., Braine J., Schinnerer E., Walter F., Colina L., 2011, A&A, 528, A124
- Combes F., García-Burillo S., Braine J., Schinnerer E., Walter F., Colina L., 2013, A&A, 550, A41
- Coppin K. E. K. et al., 2007, ApJ, 665, 936
- Cox P. et al., 2002, A&A, 387, 406
- Curran S. J., 2010, MNRAS, 402, 2657
- Curran S. J., 2012, ApJ, 748, L18
- Curran S. J., Darling J. K., Bolatto A. D., Whiting M. T., Bignell C., Webb J. K., 2007, MNRAS, 382, L11
- Curran S. J., Johansson L. E. B., Bergman P., Heikkilä A., Aalto S., 2001, A&A, 367, 457
- Curran S. J., Kanekar N., Darling J. K., 2004a, Science with the Square Kilometer Array, New Astronomy Reviews 48, Carilli C. L., Rawlings S., eds., Elsevier, Amsterdam, pp. 1095–1105
- Curran S. J., Koribalski B. S., Bains I., 2008a, MNRAS, 389, 63
- Curran S. J., Murphy M. T., Pihlström Y. M., Webb J. K., Bolatto A. D., Bower G. C., 2004b, MNRAS, 352, 563
- Curran S. J., Rydbeck G., Johansson L. E. B., Booth R. S., 1999, A&A, 344, 767
- Curran S. J., Whiting M. T., 2010, ApJ, 712, 303
- Curran S. J., Whiting M. T., 2012, ApJ, 759, 117
- Curran S. J. et al., 2011a, MNRAS, 416, 2143
- Curran S. J. et al., 2011b, MNRAS, 413, 1165
- Curran S. J., Whiting M. T., Murphy M. T., Webb J. K., Longmore S. N., Pihlström Y. M., Athreya R., Blake C., 2006, MNRAS, 371, 431
- Curran S. J., Whiting M. T., Sadler E. M., Bignell C., 2013a, MNRAS, 428, 2053
- Curran S. J., Whiting M. T., Tanna A., Sadler E. M., Pracy M. B., Athreya R., 2013b, MNRAS, 429, 3402
- Curran S. J., Whiting M. T., Webb J. K., Athreya A., 2011c, MNRAS, 414, L26
- Curran S. J., Whiting M. T., Wiklind T., Webb J. K., Murphy M. T., Purcell C. R., 2008b, MNRAS, 391, 765
- Daddi E. et al., 2010, ApJ, 713, 686
- Daddi E. et al., 2009, ApJ, 694, 1517
- Danielson A. L. R. et al., 2011, MNRAS, 410, 1687
- Darling J. K., 2003, PhRvL, 91, 011301
- Dasyra K. M., Combes F., 2012, A&A, 541, L7
- De Breuck C., Downes D., Neri R., van Breugel W., Reuland M., Omont A., Ivison R., 2005, A&A, 430, L1
- De Breuck C. et al., 2003a, A&A, 401, 911
- De Breuck C., Neri R., Omont A., 2003b, New Astronomy Review, 47, 285
- Downes D., Neri R., Wiklind T., Wilner D. J., Shaver P. A., 1999, ApJ, 513, L1
- Emonts B. H. C. et al., 2011, ApJ, 734, L25
- Emonts B. H. C. et al., 2013, MNRAS, 430, 3465
- Emonts B. H. C. et al., 2014, MNRAS, 438, 2898
- Frayser D. T. et al., 2011, ApJ, 726, L22
- Frayser D. T. et al., 1999, ApJ, 514, L13
- Freundlich J. et al., 2013, A&A, 553, A130
- Fynbo J. P. U. et al., 2011, MNRAS, 413, 2481
- Genzel R., Cesarsky C. J., 2000, Ann. Rev. Astr. Ap., 38, 761
- Genzel R. et al., 2015, ApJ, 800, 20
- Geréb K., Maccagni F. M., Morganti R., Oosterloo T. A., 2015, A&A, 575, 44
- Grasha K., Darling J., 2011, in American Astronomical Society Meeting Abstracts, Vol. 43, p. 345.02
- Greve T. R. et al., 2005, MNRAS, 359, 1165
- Greve T. R., Ivison R. J., Papadopoulos P. P., 2003, ApJ, 599, 839
- Guimarães R., Noterdaeme P., Petitjean P., Ledoux C., Srianand R., López S., Rahmani H., 2012, AJ, 143, 147

- Gupta N., Saikia D. J., 2006a, MNRAS, 370, L80
- Gupta N., Saikia D. J., 2006b, MNRAS, 370, 738
- Gupta N., Salter C. J., Saikia D. J., Ghosh T., Jeyakumar S., 2006, MNRAS, 373, 972
- Hainline L. J., Scoville N. Z., Yun M. S., Hawkins D. W., Frayer D. T., Isaak K. G., 2004, ApJ, 609, 61
- Iono D. et al., 2006, PASJ, 58, 957
- Ishwara-Chandra C. H., Dwarkanath K. S., Anantharamaiah K. R., 2003, JAA&A, 24, 37
- Iverson R. J. et al., 2012, MNRAS, 425, 1320
- Kalberla P. M. W., Kerp J., 2009, Ann. Rev. Astr. Ap., 47, 27
- Kanekar N., Briggs F. H., 2003, A&A, 412, L29
- Kanekar N. et al., 2005, PhRvL, 95, 261301
- Kanekar N., Chengalur J. N., 2002, A&A, 381, L73
- Kanekar N., Chengalur J. N., de Bruyn A. G., Narasimha D., 2003, MNRAS, 345, L7
- Kanekar N., Chengalur J. N., Lane W. M., 2007, MNRAS, 375, 1528
- Kanekar N., Prochaska J. X., Ellison S. L., Chengalur J. N., 2009, MNRAS, 396, 385
- Kennicutt, Jr. R. C., 1998, ApJ, 498, 541
- Klamer I. J., Ekers R. D., Sadler E. M., Hunstead R. W., 2004, ApJ, accepted (astro-ph/0408015)
- Klamer I. J., Ekers R. D., Sadler E. M., Weiss A., Hunstead R. W., De Breuck C., 2005, ApJ, 621, L1
- Kneib J., Neri R., Smail I., Blain A., Sheth K., van der Werf P., Knudsen K. K., 2005, A&A, 434, 819
- Koribalski B., 1996, in Minnesota Lectures on Extragalactic HI, Skillman E., ed., Vol. 106, ASP Conf. Ser., p. 238
- Krumholz M. R., McKee C. F., Tumlinson J., 2008, ApJ, 689, 865
- Krumholz M. R., McKee C. F., Tumlinson J., 2009, ApJ, 693, 216
- Lestrade J.-F., Combes F., Salomé P., Omont A., Bertoldi F., André P., Schneider N., 2010, A&A, 522, L4
- Lupu R. E. et al., 2012, ApJ, 757, 135
- Madau P., Pozzetti L., Dickinson M., 1998, ApJ, 498, 106
- Magdis G. E. et al., 2012, ApJ, 758, L9
- Magnelli B. et al., 2012, A&A, 548, A22
- Maiolino R. et al., 2007, A&A, 472, L33
- Mauch T., Sadler E. M., 2007, MNRAS, 375, 931
- McKee C. F., Krumholz M. R., 2010, ApJ, 709, 308
- Mirabel I. F., 1989, ApJ, 340, L13
- Moore C. B., Carilli C. L., Menten K. M., 1999, ApJ, 510, L87
- Morganti R., Oosterloo T. A., Tadhunter C. N., van Moorsel G., Killeen N., Wills K. A., 2001, MNRAS, 323, 331
- Morganti R., Sadler E. M., Curran S., 2015, Advancing Astrophysics with the Square Kilometre Array (AASKA14), 134
- Neri R. et al., 2003, ApJ, 597, L113
- Nesvadba N. P. H. et al., 2009, MNRAS, 395, L16
- Noterdaeme P., Srianand R., Rahmani H., Petitjean P., Pâris I., Ledoux C., Gupta N., López S., 2015, A&A, 577, A24
- Omont A., Petitjean P., Guilloteau S., McMahon R. G., Solomon P. M., Pécontal E., 1996, Nat, 382, 428
- Pannella M. et al., 2015, ApJ, 807, 141
- Papadopoulos P. P., Isaak K. G., van der Werf P. P., 2007, ApJ, 668, 815
- Papadopoulos P. P., Röttgering H. J. A., van der Werf P. P., Guilloteau S., Omont A., van Breugel W. J. M., Tilanus R. P. J., 2000, ApJ, 528, 626
- Peck A. B., Taylor G. B., Conway J. E., 1999, ApJ, 521, 103
- Peck A. B., Taylor G. B., Fassnacht C. D., Readhead A. C. S., Vermeulen R. C., 2000, ApJ, 534, 104
- Pfenniger D., Combes F., 1994, A&A, 285, 94
- Pfenniger D., Combes F., Martinet L., 1994, A&A, 285, 79
- Pihlström Y. M., Conway J. E., Vermeulen R. C., 2003, A&A, 404, 871
- Rawlings S., Abdalla F. B., Bridle S. L., Blake C. A., Baugh C. M., Greenhill L. J., van der Hulst J. M., 2004, Science with the Square Kilometer Array, New Astronomy Reviews 48, Carilli C. L., Rawlings S., eds., Elsevier, Amsterdam, pp. 1013–1027
- Reimers D., Baade R., Quast R., Levshakov S. A., 2003, A&A, 410, 785
- Riechers D. A., 2011, ApJ, 730, 108
- Riechers D. A. et al., 2010, ApJ, 720, L131
- Ries P. A., 2012, PhD thesis, University of Virginia
- Saintonge A. et al., 2013, ApJ, 778, 2
- Salter C. J., Saikia D. J., Minchin R., Ghosh T., Chandola Y., 2010, ApJ, 715, L117
- Sanders D. B., Mirabel I. F., 1996, Ann. Rev. Astr. Ap., 34, 749
- Schneider D. P. et al., 2007, AJ, 134, 102
- Solomon P. M., Vanden Bout P. A., 2005, Ann. Rev. Astr. Ap., 43, 677
- Spitzer, Jr. L., 1948, ApJ, 107, 6
- Srianand R., Gupta N., Petitjean P., Noterdaeme P., Ledoux C., 2010, MNRAS, 405, 1888
- Srianand R., Gupta N., Petitjean P., Noterdaeme P., Ledoux C., Salter C. J., Saikia D. J., 2012, MNRAS, 421
- Strong A. W. et al., 1988, A&A, 207, 1
- Tacconi L. J. et al., 2010, Nat, 463, 781
- Tacconi L. J. et al., 2006, ApJ, 640, 228
- Tacconi L. J. et al., 2013, ApJ, 768, 74
- Tanna A., Curran S. J., Whiting M. T., Webb J. K., Bignell C., 2013, ApJ, 772, L25
- Uson J. M., Bagri D. S., Cornwell T. J., 1991, PhRvL, 67, 3328
- van Gorkom J. H., Knapp G. R., Ekers R. D., Ekers D. D., Laing R. A., Polk K. S., 1989, AJ, 97, 708
- Vermeulen R. C. et al., 2003, A&A, 404, 861
- Visser R., van Dishoeck E. F., Black J. H., 2009, A&A, 503, 323
- Weiß A., Henkel C., Downes D., Walter F., 2003, A&A, 409, L41
- Weiß A., Ivison R. J., Downes D., Walter F., Cirasuolo M., Menten K., 2009, ApJ, 705, L45
- Wiklind T., Combes F., 1994, A&A, 286, L9
- Wiklind T., Combes F., 1995, A&A, 299, 382
- Wiklind T., Combes F., 1996a, Nat, 379, 139
- Wiklind T., Combes F., 1996b, A&A, 315, 86
- Wiklind T., Combes F., 1997, A&A, 328, 48
- Wiklind T., Combes F., 1998, ApJ, 500, 129
- Willott C. J., Martínez-Sansigre A., Rawlings S., 2007, AJ, 133, 564
- Yan L. et al., 2010, ApJ, 714, 100